POLITECNICO
MILANO 1863

Course of Spacecraft Attitude Dynamics and Control

Prof. Franco Bernelli Zazzera

Final project

David Reina 953171

Academic Year 2020-2021

Contents

1 Introduction

In this report the design of the Attitude Dynamics and Control System of a 12 U CubeSat is carried out. The satellite, that is required to point Earth with a pointing error less than 1°, has been considered on a LEO orbit, therefore the simulation takes into account the most prominent disturbance torques typical of this environment as well as the performances of the selected ADCS components.

1.1 Satellite configuration

The CubeSat configuration is reported in Figure 1: the spacecraft consists of a 3 $U \times 2\ U \times 2\ U$ main body and a pair of 5 $U \times 2\ U$ solar panels, where 1 U refers to 10 cm.

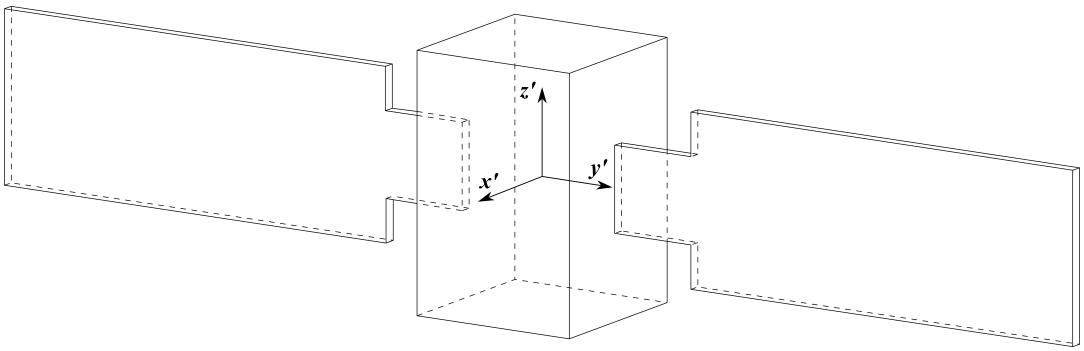

Figure 1: The 12U CubeSat scheme

The reference frame $\{x', y', z'\}$ is considered with each axis parallel to the principal axis of inertia, while the body frame $\{x, y, z\}$ is the principal inertia frame centered on the Center of Gravity (CG) of the spacecraft. The CG coordinates in the reference frame are:

$$r'_{CG} = \{1.8,\ 0,\ 0\}^T \quad cm \tag{1}$$

The inertia matrix of the satellite, including the deployed solar panels, is:

$$I = \begin{bmatrix} 91.6 & 0 & 0 \\ 0 & 25.1 & 0 \\ 0 & 0 & 100.9 \end{bmatrix} \cdot 10^{-2} \quad kg \cdot m^2 \tag{2}$$

1.2 Orbit design

The LEO orbit of the CubeSat is characterized by the nominal parameters reported in Table 1.

Parameter	Value
a	7171 km
e	0.1
i	98.62°
Ω	0°
ω	0°

Table 1: Orbit parameters

where a is the semi-major axis, e is the eccentricity, i is the inclination, Ω is the right ascension of the ascending node and ω is the argument of perigee.

1.3 Sensors

The satellite is equipped with a gyroscope, a Sun sensor and an Earth horizon sensor. In the following sections are reported the technical parameters of the selected sensors.

1.3.1 Gyroscope - STIM300 *[Sensonor]*

ARW	RRW	Sampling frequency	Power	Dimensions	Mass
$0.15°/\sqrt{h}$	$0.0003°/\sqrt{h^3}$	262 Hz	1.5 W	$44.8 \times 38.6 \times 21.5$ mm	55 g

Table 2: Gyroscope specifications [1]

1.3.2 Sun sensor - nanoSSOC-D60 *[SolarMems Technologies]*

Accuracy	FOV	Sampling frequency	Power	Dimensions	Mass
$< 0.5°$	$\pm 60°$	50 Hz	< 76 mW	$43 \times 14 \times 5.9$ mm	6.2 g

Table 3: Sun sensor specifications [2]

1.3.3 Earth horizon sensor - MAI-SES *[Maryland Aerospace]*

Accuracy	FOV	Voltage	Dimensions	Mass
$< 0.25°$	$> 7°$	3.3 V	$43.26 \times 31.75 \times 31.75$ mm	33 g

Table 4: Earth horizon sensor specifications [3]

1.4 Actuators

The satellite is equipped with a set of 12 variable thrust electrical thrusters. In the following section are reported the technical parameters of the selected actuators.

1.4.1 Attitude thrusters - NANO IR^3 *[Enpulsion Spacecraft Technology]*

Type	Thrust range	I_{sp} range	Power
FEEP	$10 - 500$ μN	$1500 - 4000$ s	$8 - 45W$

Table 5: Electrical thrusters specifications [4]

2 Model description

2.1 Attitude dynamics

The attitude dynamics of the satellite, which is considered as a rigid body, are computed using the Euler's equation [5]:

$$\mathbf{I}\,\dot{\underline{\omega}} = \mathbf{I}\,\underline{\omega} \times \underline{\omega} + \underline{M}_d + \underline{M}_c \tag{3}$$

where $\underline{\omega}$ is the angular velocity, $\underline{M}_d$ is the disturbing torque and $\underline{M}_c$ is the control torque. The numerical integration of this equation is then used to compute the spacecraft kinematics using as attitude parameters the Euler's angles ϕ, θ, and ψ [5] to obtain the attitude matrix. In particular, for this study the set $\mathbf{A_{313}}(\phi, \theta, \psi)$ is chosen which considers two rotations around the z axis and the middle one around the x axis of the inertial reference frame.
The Euler angles from this set can be computed integrating:

$$\begin{cases} \dot{\phi} = \frac{(\omega_x \sin\psi + \omega_y \cos\psi)}{\sin\theta} \\ \dot{\theta} = \omega_x \cos\psi - \omega_y \sin\psi \\ \dot{\psi} = \omega_z - (\omega_x \sin\psi + \omega_y \cos\psi)\frac{\cos\theta}{\sin\theta} \end{cases} \tag{4}$$

while, the $\mathbf{A_{313}}(\phi, \theta, \psi)$ can be computed as:

$$\mathbf{A_{313}} = \begin{bmatrix} \cos\psi\cos\phi - \sin\psi\sin\phi\cos\theta & \cos\psi\sin\phi + \sin\psi\cos\phi\cos\theta & \sin\psi\sin\theta \\ -\sin\psi\cos\phi - \cos\psi\sin\phi\cos\theta & -\sin\psi\sin\phi + \cos\psi\cos\phi\cos\theta & \cos\psi\sin\theta \\ \sin\phi\sin\theta & -\cos\phi\sin\theta & \cos\theta \end{bmatrix} \tag{5}$$

Using the Euler angles as attitude parameters it is important to consider the singularities that this decision brings. In fact, in this case, when $\theta = k\pi$ the inverse of the rotation matrix isn't defined. Therefore, along with the computation of the $\mathbf{A_{313}}$ matrix, also the $\mathbf{A_{312}}(\phi, \theta, \psi)$ is computed, so that, when the θ angle of the 313 set comes close to $k\pi$, the $\mathbf{A_{312}}$ is used instead of the $\mathbf{A_{313}}$. This can be performed because the singularities for $\mathbf{A_{312}}$ happen when $\theta = (2\,k + 1)\frac{\pi}{2}$. The Euler angles of the 312 set can be obtained integrating:

$$\begin{cases} \dot{\phi} = \frac{(\omega_y \cos\psi - \omega_x \sin\psi)}{\cos\theta} \\ \dot{\theta} = \omega_x \cos\psi + \omega_z \sin\psi \\ \dot{\psi} = \omega_y - (\omega_z \cos\psi - \omega_x \sin\psi)\frac{\sin\theta}{\cos\theta} \end{cases} \tag{6}$$

while the $\mathbf{A_{312}}(\phi, \theta, \psi)$ can be computed as:

$$\mathbf{A_{312}} = \begin{bmatrix} \cos\psi\cos\phi - \sin\psi\sin\phi\sin\theta & \cos\psi\sin\phi + \sin\psi\cos\phi\sin\theta & -\sin\psi\cos\theta \\ -\sin\phi\cos\theta & -\cos\phi\cos\theta & \sin\theta \\ \sin\psi\cos\phi + \cos\psi\sin\phi\sin\theta & \sin\psi\sin\phi - \cos\psi\cos\phi\sin\theta & \cos\psi\cos\theta \end{bmatrix} \tag{7}$$

2.2 Disturbing torques

The disturbing torques considered for this study are the Earth's magnetic field torque, the solar radiation pressure torque and the gravity gradient torque. The total disturbing torque is therefore computed as the summation of these contributions:

$$\underline{M}_d = \underline{M}_{MAG} + \underline{M}_{SRP} + \underline{M}_{GG} \tag{8}$$

Note that the disturbing torque due to atmospheric drag isn't considered because for orbit altitudes higher than 700 km its magnitude is negligible [5].
In order to compute these contributions the position vector of the satellite along its orbit is needed. In particular, the integration of the orbit has been performed neglecting the effect of orbital perturbations, therefore it is possible to integrate the true anomaly using:

$$\dot{\theta} = \frac{n(1 + e \cdot \cos\theta)^2}{(1 - e^2)^{3/2}} \tag{9}$$

where n is the orbital mean motion defined as: $n = \sqrt{\frac{\mu}{a^3}}$, where μ is Earth's gravitational parameter. It's then possible to compute the position vector in the inertial frame $\underline{r}$ using the orbit parameters already defined. After obtaining the true anomaly, it is possible to define the rotation matrix from the inertial to the Local Vertical Local Horizontal frame (LVLH) [5]:

$$\mathbf{A_{L/N}} = \begin{bmatrix} \cos\theta & \sin\theta & 0 \\ -\sin\theta & \cos\theta & 0 \\ 0 & 0 & 1 \end{bmatrix} \begin{bmatrix} 1 & 0 & 0 \\ 0 & \cos i & \sin i \\ 0 & -\sin i & \cos i \end{bmatrix} \tag{10}$$

2.2.1 Earth's magnetic field

It is possible to obtain the disturbing torque generated by Earth's magnetic field using a simplified model that considers the magnetic field as one generated by a dipole [5]. The field vector can be computed as:

$$\underline{b}_N = \frac{R_E^3 H_0}{||\underline{r}||^3}[3(\underline{\hat{m}} \cdot \underline{\hat{r}})\underline{\hat{r}} - \underline{\hat{m}}] \tag{11}$$

where R_E is Earth's radius, $\underline{\hat{r}}$ is a versor in the direction of $\underline{r}$, $\underline{\hat{m}}$ is a versor in the direction of the magnetic field that can be computed as:

$$\underline{\hat{m}} = \begin{bmatrix} \sin 11.5^\circ \cos\omega_E t \\ \sin 11.5^\circ \sin\omega_E t \\ \cos 11.5^\circ \end{bmatrix} \tag{12}$$

with ω_E as Earth's angular velocity around its axis. At last H_0 is a term obtained from the first order Gaussian coefficients reported by the International Geomagnetic Reference Field (IGRF):

$$H_0 = \sqrt{(g_0^1)^2 + (g_1^1)^2 + (h_1^1)^2} \tag{13}$$

The torque can therefore be computed as:

$$\underline{M}_{MAG} = \underline{M} \times \mathbf{A_{B/N}}\underline{b}_N = \underline{M} \times \underline{b}_B \quad \underline{M} = \{0.1,\ 0.5,\ 0.1\}^T A/m^2 \tag{14}$$

where $\underline{M}$ is the residual dipole of the satellite due to on-board currents, while $\underline{b}_N$ and $\underline{b}_B$ are the field vector in the inertial and body frame.

2.2.2 Solar radiation pressure

The electromagnetic radiation illuminating the outer surfaces of the satellite creates a pressure that generates a torque around the CG of the satellite [5]. The main contributions of this radiation, considering an average altitude of the satellite equal to 800 km, are reported in Table 6.

Direct solar radiation	**Radiation reflected by Earth**	**Earth radiation**	F_e
1358 W/m^2	540 W/m^2	130.2 W/m^2	2028.2 W/m^2

Table 6: Radiation contributions

In order to compute the torque generated by the incoming radiation, the CubeSat surface has been divided into flat surfaces associated with a given specular and diffuse reflection coefficients (ρ_s, ρ_d): in particular for solar panels $\rho_s = 0.8$, for the central body $\rho_s = 0.5$ and $\rho_d = 0.1$ for all the surfaces.
The Sun position has been computed using a simplified model such as the Sun direction in the body frame is:

$$\underline{\hat{S}}_B = \mathbf{A_{B/N}}\underline{\hat{S}}_N = \mathbf{A_{B/N}} \begin{Bmatrix} \cos(n_{Sun}t) \\ \sin(n_{Sun}t)\cos(23.45°) \\ \sin(n_{Sun}t)\sin(23.45°) \end{Bmatrix} \tag{15}$$

where $n_{sun} = 2\pi/1year$.

The force acting on each of the N_{surf} surfaces is obtained as:

$$\underline{F}_i = -\frac{F_e}{c}A_i(\underline{\hat{S}}_B \cdot \underline{\hat{n}}_{B,i})\left\{(1-\rho_{s,i})\underline{\hat{S}}_B + \left[2\rho_{s,i}(\underline{\hat{S}}_B \cdot \underline{\hat{n}}_{B,i}) + \frac{2}{3}\rho_{d,i}\right]\underline{\hat{n}}_{B,i}\right\} \quad i = 1, ..., N_{surf} \tag{16}$$

Note that this computation is performed only for those surfaces for which $\underline{\hat{S}}_B \cdot \underline{\hat{n}}_{B,i} > 0$. For the sake of simplicity, in the computation of this disturbing torque the solar panels are assumed to be fixed parallel to the vertical faces of the main body, as shown in Figure 1. The disturbing torque can at last be computed as:

$$\underline{M}_{SRP} = \sum_{i=1}^{N_{surf}} \underline{r}_i \times \underline{F}_i \tag{17}$$

2.2.3 Gravity gradient

The torque generated by the gravity gradient can be obtained as [5]:

$$\underline{M}_{GG} = \frac{3\mu}{||\underline{r}||^3} \begin{Bmatrix} (I_z - I_y)c_2c_3 \\ (I_x - I_z)c_1c_3 \\ (I_y - I_x)c_2c_1 \end{Bmatrix} \tag{18}$$

where: $\{c_1,\ c_2,\ c_3,\}^T = \mathbf{A_{B/N}}\mathbf{A_{L/N}}^T\{1,\ 0,\ 0,\}^T = \mathbf{A_{B/L}}\{1,\ 0,\ 0,\}^T$.

2.3 Sensors

2.3.1 Gyroscope

The measurements performed by the gyroscope have been modeled considering the inevitable presence of noise. In particular, gyroscopes are characterized by the angular random walk (ARW) due to thermo-mechanical noise of the system and by the rate random walk (RRW) due to electronic noise (flicker). These values have been retrieved by the data sheet of the chosen gyroscope and used to model these two contributions as Gaussian noises ($\underline{n}$ and $\underline{b}$ respectively) with zero mean value and using as standard deviations $ARW/\sqrt{t_s}$ and $RRW/\sqrt{t_s}$ where t_s is the sampling time [6]:

$$\underline{\omega}_{raw} = \underline{\omega} + \underline{n} + \underline{b} \quad \underline{n} = \sigma_n\chi_n \quad \dot{\underline{b}} = \sigma_b\chi_b \tag{19}$$

2.3.2 Earth horizon and Sun sensors

The behaviour of these sensors haven't been simulated as the gyroscope, instead the measurements made by these sensors have been modeled as the real values obtained from the propagation of the orbit and from the attitude kinematics summed with a Gaussian noise with amplitude related to the sensor accuracy reported in Tables 3 and 4. The measurement vectors have been computed as:

$$\underline{\hat{v}}_{B_i} = \mathbf{A}_\epsilon\mathbf{A_{B/N}}\underline{\hat{v}}_{N_i} \tag{20}$$

where $\mathbf{A}_\epsilon$ is the error matrix related to the sensors, while $\underline{\hat{v}}_{B_i}$ and $\underline{\hat{v}}_{N_i}$ are the measurements vectors respectively in body and inertial frame. The measurements considered are the Sun direction versor $\underline{\hat{S}}_N$, obtained from the Sun sensor, and the position vector of the satellite $\underline{r}$, obtained from the Earth horizon sensor.

2.4 Actuators

The only type of actuator used in the system is variable thrust jets. In particular, electric thrusters have been chosen, due to their ease of modulation in amplitude, and their high specific impulse that allows a reduced propellant consumption. The chosen model can produce a variable thrust from as low as 10 μN to 500 μN, therefore it can provide fine adjustments and limits overshooting, although this inevitably increases the response time of the system when higher control torques are needed.
The configuration used is typical for electric propulsion attitude system [5], and involves 12 units arranged in the lower part of the satellite as shown in Figure 2 so that the rotations around the three axis are controlled by 4 thrusters each. Even if the configuration isn't symmetrical with respect to the centre of mass, due to the low thrust, the residual force can be neglected.

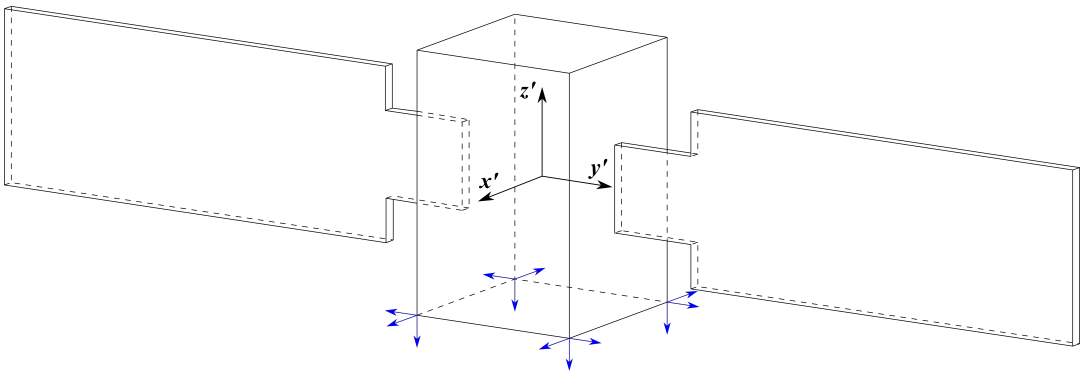

Figure 2: Thrusters configuration scheme

The torque generated by the actuators can be computed as:

$$\underline{M_{c}}_{real} = [\hat{\mathbf{R}}]\underline{u}_{c_{real}} \tag{21}$$

where $[\hat{\mathbf{R}}]$ is the thruster configuration matrix which maps the torque action of each thruster and it's computed as shown in Equation 22, while $\underline{u}_{c_{real}}$ is a vector that expresses the thrust allocated for each thruster.

$$[\hat{\mathbf{R}}] = \left\{\underline{r}_1 \times \underline{\hat{f}}_1 \quad \dots \quad \underline{r}_{12} \times \underline{\hat{f}}_{12}\right\} \tag{22}$$

In order to obtain $\underline{u}_{c_{real}}$, first of all the ideal control torque needs to be computed using a simple "bang-bang" type controller [6]:

$$\underline{M}_{c_{ideal}} = -\underline{T}sgn(\underline{S}) \tag{23}$$

where $\underline{S}$ depends on each mission phase. Note that this controller type is similar to one used for fixed thrust jets, with the only exception that $\underline{T}$ corresponds to an ideal torque proportional to $\underline{S}$. In addition, the computation of $\underline{T}$ follows a Schmitt-Trigger logic. Next, due to the fact that in general the Moore-Penrose pseudo inverse cannot be used to solve $-[\hat{\mathbf{R}}]\underline{u}_c = \underline{M}_{c_{ideal}}$ because of the additional constraint of $\underline{u}_c \geqslant 0$, it is possible to use a general pseudo inverse defined as:

$$\underline{u}_c = -[\hat{\mathbf{R}}]^{+}\underline{M}_{c_{ideal}} + \gamma\underline{w} \tag{24}$$

where $\underline{w}$ is the null space vector of $[\hat{\mathbf{R}}]$, and γ is a scalar defined as $\gamma = max_{i=1,\dots,N}([\hat{\mathbf{R}}]^{+}\underline{M}_{c_{ideal}})/w_i$.
The last step is to check if the thrust allocated for each thruster expressed by $\underline{u}_c$ is constrained between the minimum and maximum thrust admissible by each actuator and then build the final vector $\underline{u}_{c_{real}}$.

3 Mission description

The objective of the satellite attitude control system is to orient the spacecraft from the initial conditions towards Earth. In particular, the x axis of the body frame is required to be aligned with the x axis of the Local Vertical Local Horizontal frame (LVLH). Therefore as the main performance parameter, the pointing error between these two versors is chosen, as:

$$\epsilon_{pointing} = \arccos[(\mathbf{A_{B/N}}\mathbf{A_{L/N}}^T\underline{\hat{x}}_L)\cdot\underline{\hat{x}}_B] \tag{25}$$

In particular the desired attitude is characterized by:

- Desired attitude matrix: $\mathbf{A_d} = \mathbf{A_{L/N}}$
- Desired angular velocity: $\underline{\omega}_d = \{0,\ 0,\ n\}^T$
- Desired performance: $\epsilon_{pointing} \leqslant 1^\circ$

The attitude system mission is then composed by three phases:

- Detumbling
- Slew manoeuvre
- Earth pointing

4 Control and determination algorithms

4.1 Attitude determination algorithm

In order to perform the attitude determination, an algorithm based on the solution of the Wabha's problem is used. In particular, this problem consists in minimizing the weighted cost function:

$$\mathbf{J} = \frac{1}{2}\sum_{i=1}^{N}\alpha_i||\underline{\hat{v}}_{B_i} - \mathbf{A_{B/N}}\underline{\hat{v}}_{N_i}||^2 \tag{26}$$

where N is the number of attitude sensors, α is a constant related to the sensor precision, $\underline{\hat{v}}_{B_i}$ and $\underline{\hat{v}}_{N_i}$ are unit vectors measured respectively in the body and in the inertial frame.
To solve the Wabha's problem, it results that the optimal solution maximizes:

$$\begin{aligned}\tilde{\mathbf{J}} &= tr(\mathbf{A_{B/N}}\mathbf{B}^T)\\ \mathbf{B} &= \sum_{i=1}^{N}\alpha_i\underline{\hat{v}}_{B_i}\hat{\underline{v}}_{N_i}^T\end{aligned} \tag{27}$$

From [6], it is possible to retrieve the attitude matrix using the single value decomposition (SVD) of $\mathbf{B}$, and then computing $\mathbf{A_{B/N}}$ using the following procedure:

$$\begin{aligned}\mathbf{B} &= \mathbf{USV}^T\\ \mathbf{M} &= diag(1,\ 1,\ (det\mathbf{U}\cdot det\mathbf{V}))\\ \mathbf{A_{B/N}} &= \mathbf{UMV}^T\end{aligned} \tag{28}$$

4.2 Detumbling

During the detumbling phase, the ADC system must reduce the spacecraft angular velocity almost to zero from the initial conditions. This is performed using the procedure described in Section 2.4. In particular, the ideal control torque expression used for detumbling involves the parameter $S = \omega$, therefore:

$$\underline{M}_{c_{ideal}} = -\underline{T} sgn(\underline{\omega}) \tag{29}$$

The parameter $\underline{T}$ is the ideal momentum couple in the three axis, and it's obtained as:

$$\underline{T} = \underline{F}\ \underline{l} \tag{30}$$

where $\underline{l}$ is the vector of the distance between the two forces, and it is expressed as:

$$\underline{l} = \begin{Bmatrix} 2 \cdot 1.5\ U \\ 2 \cdot 1\ U \\ 2 \cdot 1\ U \end{Bmatrix} \tag{31}$$

while $\underline{\mathrm{F}}$ is a function of the parameter $\underline{S}$, which in this case it's equal to $\underline{\omega}$, and indicates the amount of thrust that the thrusters need to provide to the system to detumble the satellite, and it is obtained using a Schmitt-Trigger-like logic:

$$F_i = \begin{cases} F_{max} & if \quad |S_i| > S_{max} \\ \frac{F_{max}-F_{min}}{S_{max}-S_{min}}(S_i - S_{min}) + F_{min} & if \quad S_{min} < |S_i| < S_{max} \\ 0 & if \quad |S_i| < S_{min} \end{cases} \qquad i = x, y, z \tag{32}$$

where F_{max} and F_{min} are respectively the maximum and minimum thrust available from the each thruster, while S_{max} and S_{min} are arbitrary values. Regarding the detumbling these parameters have been set to: $S_{max} = 1 \cdot 10^{-2}$ and $S_{min} = 1 \cdot 10^{-4}$.

4.3 Slew manoeuvre and Earth pointing

The slew manoeuvre consists of orientating the satellite to the desired alignment, while in the pointing phase, the spacecraft must be kept in the desired alignment for the duration of the mission. In the case of this study, the desired attitude coincides with the Local Vertical Local Horizontal frame, therefore the body frame must match the LVLH frame as much precisely as possible. In addition, the angular velocity during the pointing phase must be the same of the LVLH frame. Therefore the desired angular velocity and attitude matrix are:

$$\underline{\omega}_d = \{0, 0, n\}^T \qquad \mathbf{A_d} = \mathbf{A_{L/N}} \tag{33}$$

The same procedure explained in Section 2.4 is used, however in this case the parameter S is the tracking control obtained using Lyapunov control function [6]:

$$\underline{S} = -[-k_1 \underline{\omega}_e - k_2(\mathbf{A_e}^T - \mathbf{A_e})^V + \underline{\omega} \times \mathbf{I}\underline{\omega} + \mathbf{I}(\mathbf{A_e}\dot{\underline{\omega}}_d - [\underline{\omega}_e]^\wedge \mathbf{A_e}\underline{\omega}_d)] \tag{34}$$

with $\underline{\omega}_e = \underline{\omega} - \mathbf{A_e}\underline{\omega}_d$, $\mathbf{A_e} = \mathbf{A_{B/N}}\mathbf{A_e}$ and $(\mathbf{A_e}^T - \mathbf{A_e})^V = \{A_{e_{2,3}} - A_{e_{3,2}}, A_{e_{3,1}} - A_{e_{1,3}}, A_{e_{1,2}} - A_{e_{2,1}}, \}^T$. The values of the tuning parameters k_1 and k_2 used for the slew manoeuvre and Earth pointing vary between the two phases, in particular:

- Slew manoeuvre: $k_1 = 1$, $k_2 = 0.0085$
- Earth pointing: $k_1 = 1$, $k_2 = 0.02$

In order to obtain the value of $\underline{T}$, the same procedure explained in Section 4.2 is performed, however for the slew manoeuvre and Earth pointing the values of $S_{max} = 1 \cdot 10^{-3}$ and $S_{min} = 3 \cdot 10^{-6}$ have been used.

4.4 Noise filtering

A state observer is used to filter noise out from the raw measured gyro angular velocity. In particular the following equation has been used:

$$\mathbf{I}\,\dot{\underline{\omega}}_{est} = \mathbf{I}\,\underline{\omega}_{est} \times \underline{\omega}_{est} + \underline{M}_d + \underline{M}_c + \alpha(\underline{\omega}_{est} - \underline{\omega}_{raw}) \tag{35}$$

with $\alpha < 0$ as tuning parameter.

5 Simulation scheme

A block scheme of the simulation is shown in Figure 3.

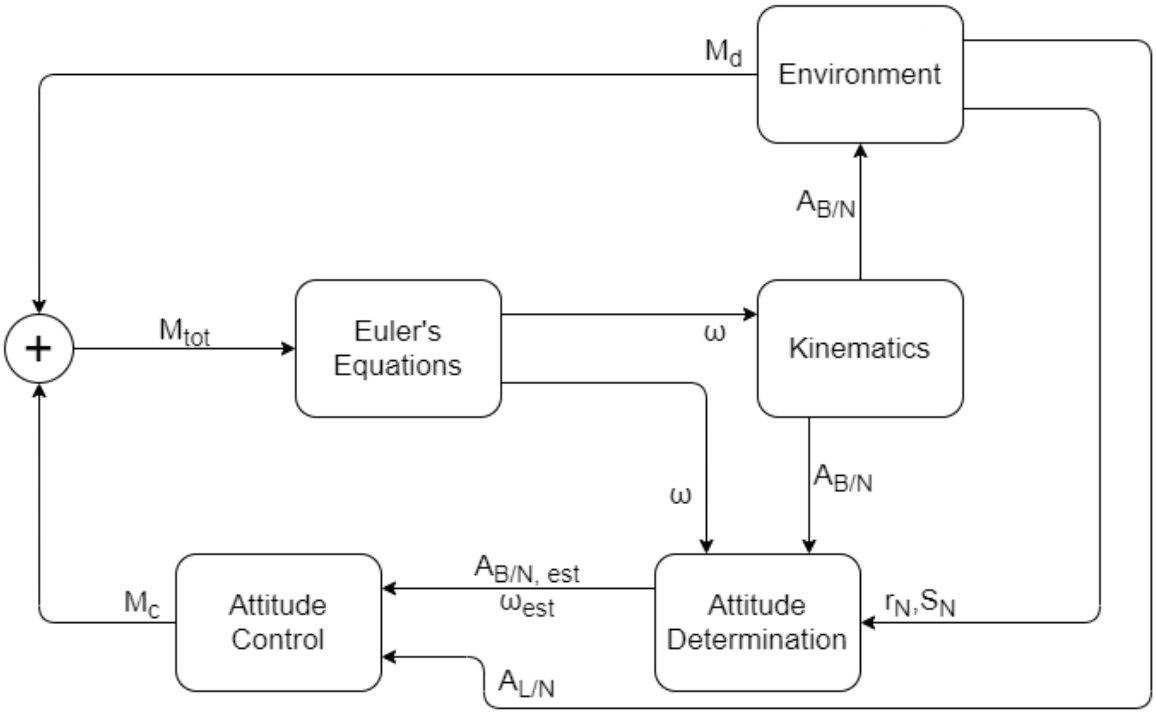

Figure 3: Simulation scheme.

6 Results

In this section are reported the attitude dynamics of the satellite obtained using Simulink models. The simulation was performed by a solver using $ode15s$ with absolute and relative tolerances equal to $1e-8$. The initial condition at $t = 0\ s$ are:

- True anomaly: $\theta(0) = 0^\circ$
- Angular velocity: $\underline{\omega}(0) = \{10, -15, 5\}^T\ deg/s$
- Euler's angles : $\underline{EA}(0) = \{9.7, 19, 6\}\ deg$

6.1 Uncontrolled dynamics

The first step of the analysis concerns the uncontrolled dynamics of the satellite during one orbital period in which the ADC system is offline.
The spacecraft attitude dynamics are affected by only the perturbing torques. The evolution of the magnitudes of this torques are reported in Figure 4.

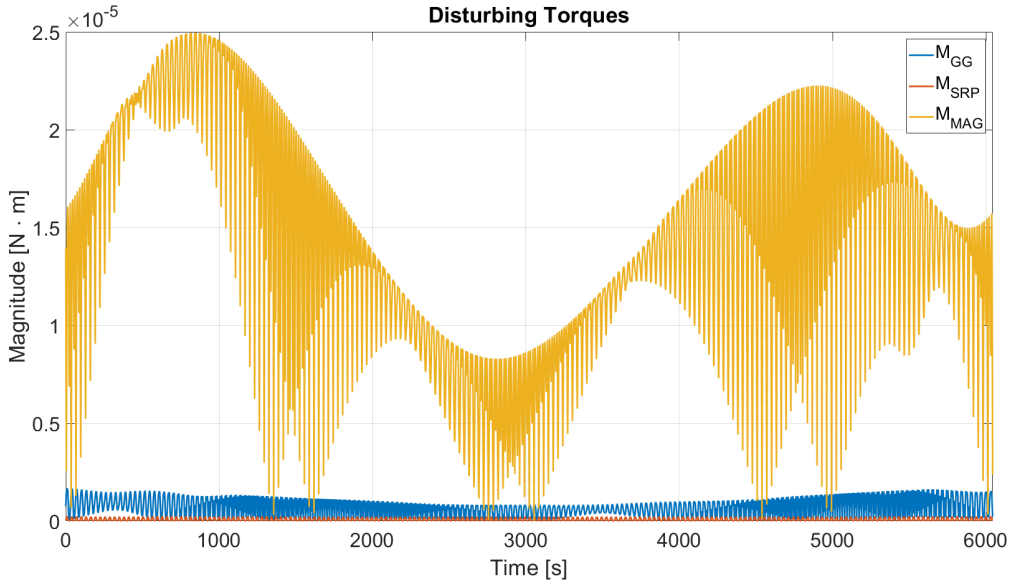

Figure 4: Disturbing torques contributions in an orbital period.

The maximum values of these perturbing torques are reported in Table 7.

	M_{GG}	M_{MAG}	M_{SRP}
Magnitude $[N\ m]$	$1.6695 \cdot 10^{-6}$	$2.4957 \cdot 10^{-5}$	$2.3883 \cdot 10^{-7}$

Table 7: Maximum values of the disturbing torques.

As expected, the main perturbing effect is due to Earth's magnetic field, due to the low altitude of the orbit.

In the following figures are reported the simulation results regarding the angular velocity components (Figure 5), the Euler's angle evolution (Figure 6) and the pointing error (Figure 7).

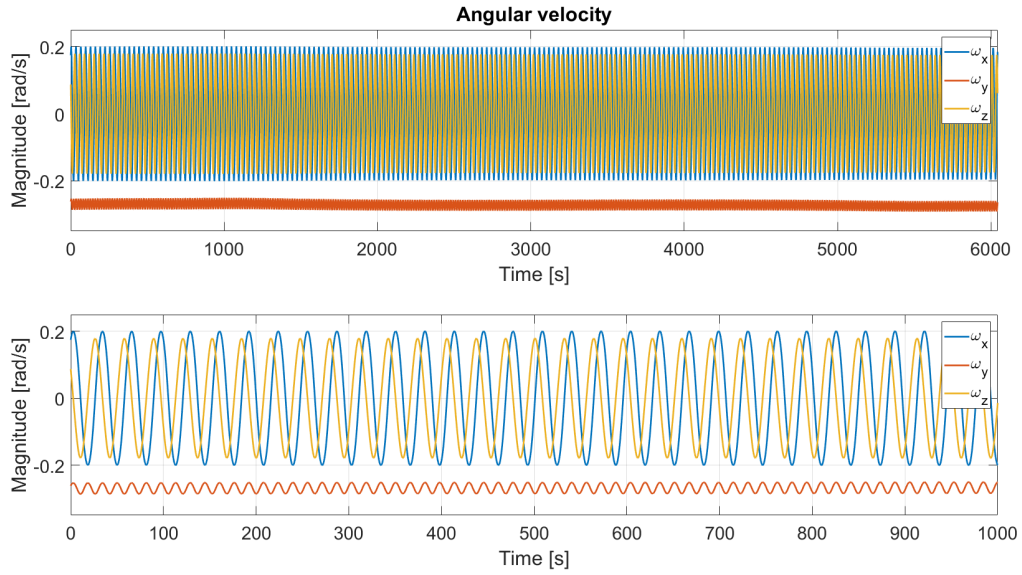

Figure 5: Angular velocity in the uncontrolled case in an orbital period and in the first 1000 seconds.

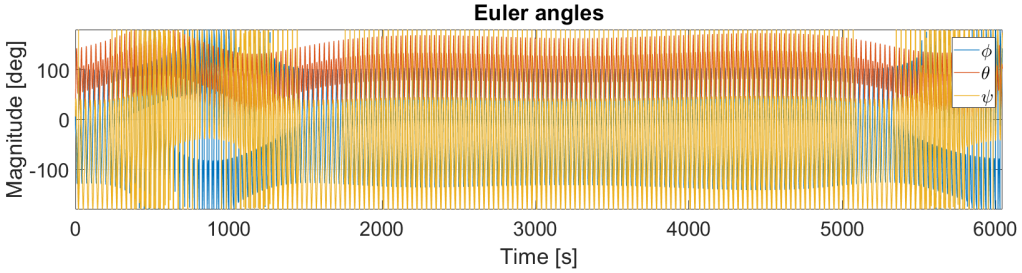

Figure 6: Euler's angle evolution in the uncontrolled case in an orbital period.

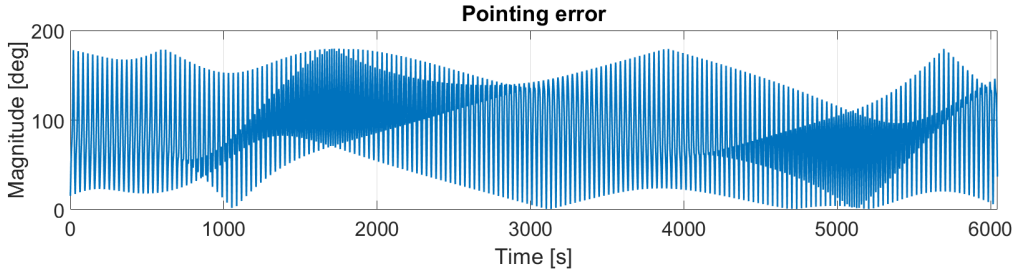

Figure 7: Pointing error in the uncontrolled case in an orbital period.

6.2 Detumbling

The detumbling simulation restarts at $t = 0\ s$, so the initial conditions are the same as the uncontrolled case, and are reported in Section 6.This phase lasts 2000 s after which an angular velocity of less than $10^{-3}\ rad/s$ is reached.
In the following figures are reported the simulation results regarding the angular velocity components (Figure 8), the Euler's angle evolution (Figure 9) and the pointing error (Figure 10).

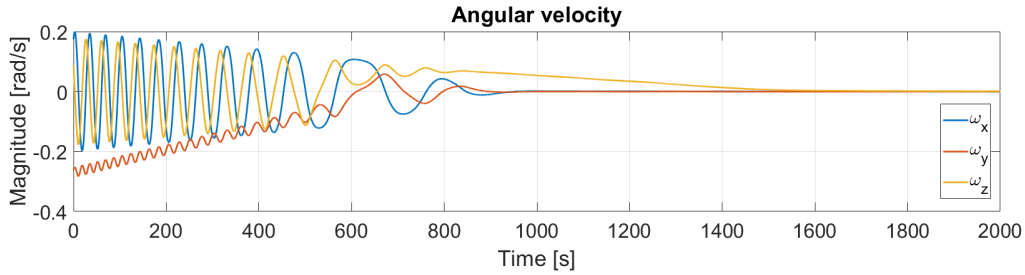

Figure 8: Angular velocity evolution during the detumbling phase.

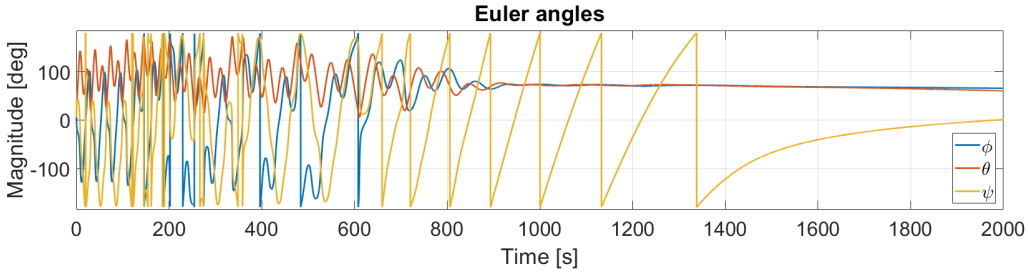

Figure 9: Euler's angle behaviour in the detumbling phase.

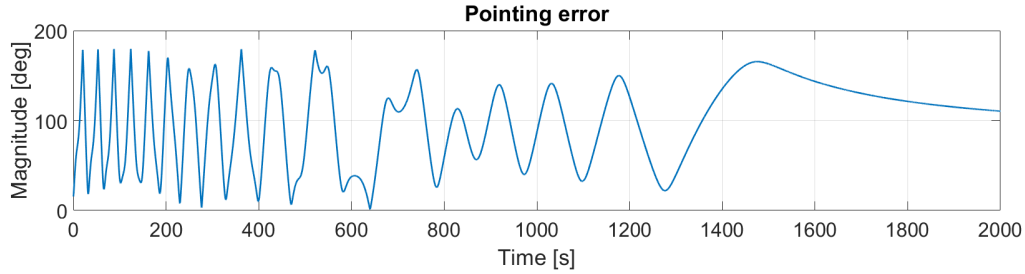

Figure 10: Pointing error in the detumbling phase.

During this phase the actuators are activated to perform the detumbling manoeuvre, therefore, in the following figures are reported some important parameters regarding them. In Figure 11 are shown the evolution of the components of the real control torque, while in Figure 12 is reported the difference between the ideal and real control torques. This error is due to the thrust limits of the thrusters especially in the first part of the phase when higher torque is needed, but eventually it goes to nearly zero. Due to the fact that the system uses variable thrust jets, their thrust level evolution is reported in Figure 13 as a percentage with respect to the maximum thrust available from each thruster.

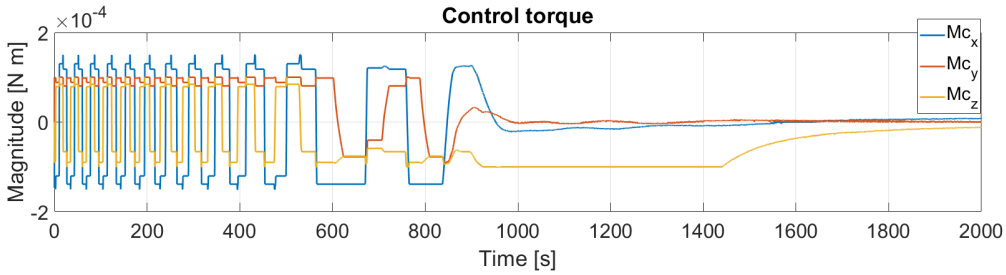

Figure 11: Control torque components during the detumbling phase.

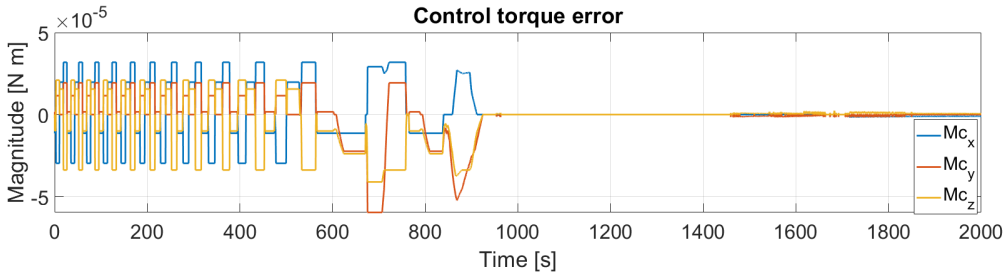

Figure 12: Ideal and real control torque differences during the detumbling phase.

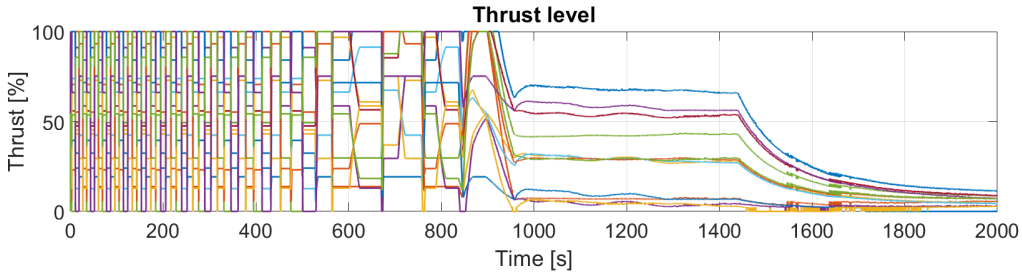

Figure 13: Thrust levels during Earth detumbling phase.

6.3 Slew manoeuvre

The slew manoeuvre starts at $t = 2000\ s$ right after the detumbling. This phase lasts for only 400 s after which the angular velocity reaches the desired value expressed in Section 3, and the attitude matrix $\mathbf{A_{B/N}}$ matches almost perfectly the desired attitude matrix $\mathbf{A_{L/N}}$.
In the following figures are reported the simulation results regarding the angular velocity components (Figure 14), the Euler's angle evolution (Figure 15) and the pointing error (Figure 16). The the attitude matrix error ($\mathbf{A_e} = \mathbf{A_{B/N}} \mathbf{A^T_{L/N}}$) is also reported in Figure 17. Note that at the end of this phase the pointing error reaches an acceptable value lower than 1° that follows the requirements set in Section 3, as well as the angular velocity converges approximately to the desired value set in Section 3, and $\mathbf{A_e}$ converges to the identity matrix.

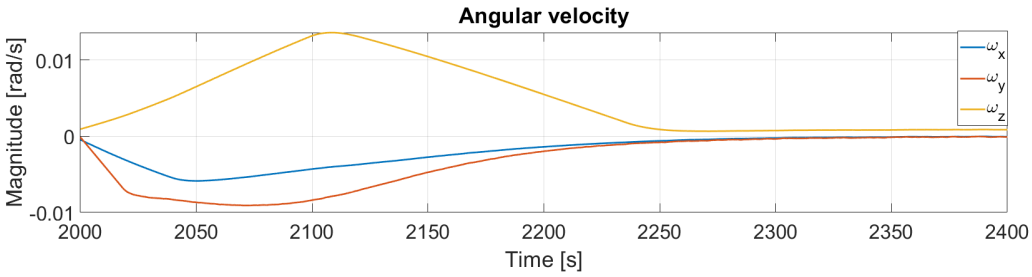

Figure 14: Angular velocity evolution during the slew manoeuvre and Earth pointing.

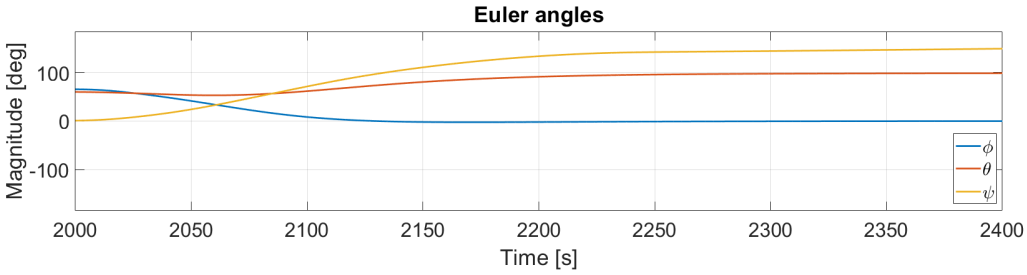

Figure 15: Euler's angles during slew manoeuvre.

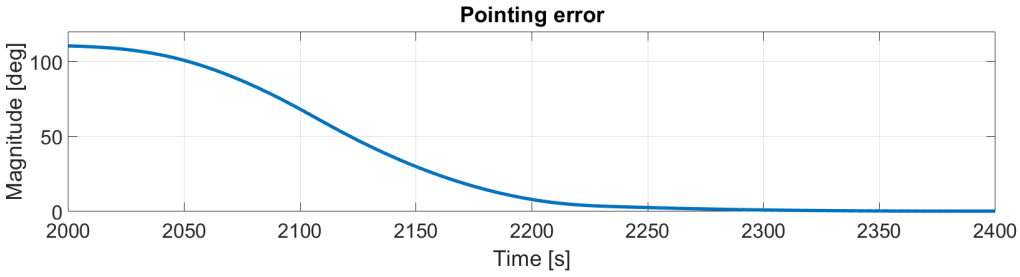

Figure 16: Pointing error during slew manoeuvre.

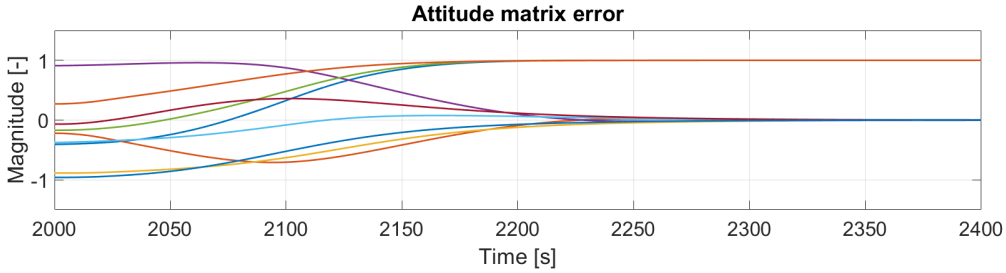

Figure 17: Attitude matrix error evolution during the slew manoeuvre.

Regarding the control torque, the real control momentum is reported in Figure 18, the difference between the real and ideal control torques is shown in Figure 19. At last, the thrust level for each actuator is plotted in Figure 20.

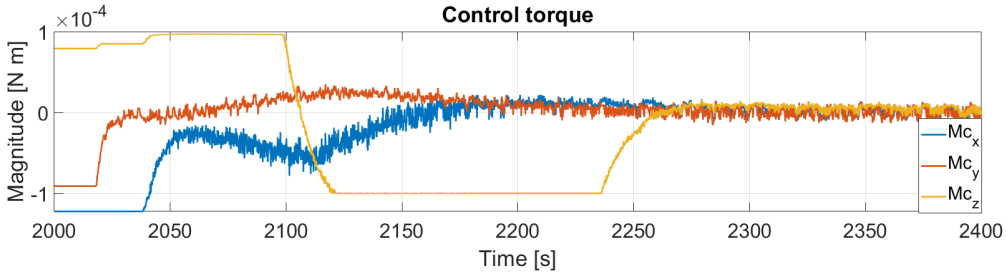

Figure 18: Control torque components during slew manoeuvre.

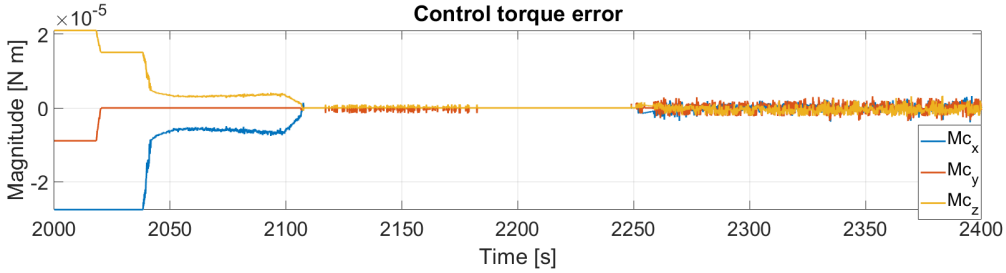

Figure 19: Ideal and real control torque differences during the slew manoeuvre.

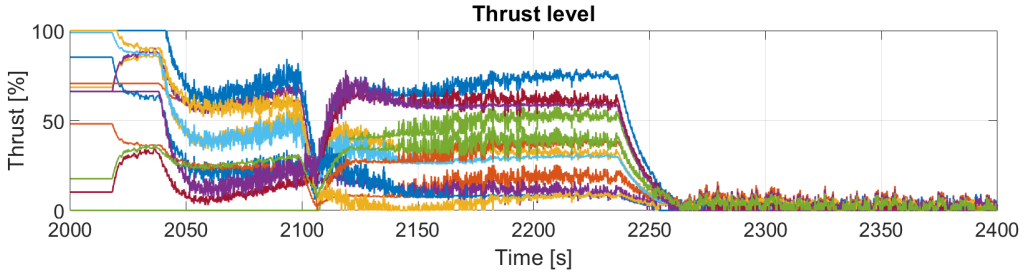

Figure 20: Thrust level during slew manoeuvre.

6.4 Earth pointing

The Earth pointing phase is the last one and also the longest. It starts right after the slew manoeuvre at $t = 2400\ s$ and lasts for the whole duration of the mission, however, this phase simulation was carried out for two orbital periods in order to verify that the mission requirements are satisfied.
In the following figures are reported the simulation results regarding the angular velocity components (Figure 21), the Euler's angle evolution (Figure 22) and the pointing error (Figure 23). The the attitude matrix error ($\mathbf{A_e}$) is also reported in Figure 24.
It's worth noticing that the mission requirements are met, in fact the pointing error stays under the 1° limit and the angular velocity oscillates very closely around the desired value.

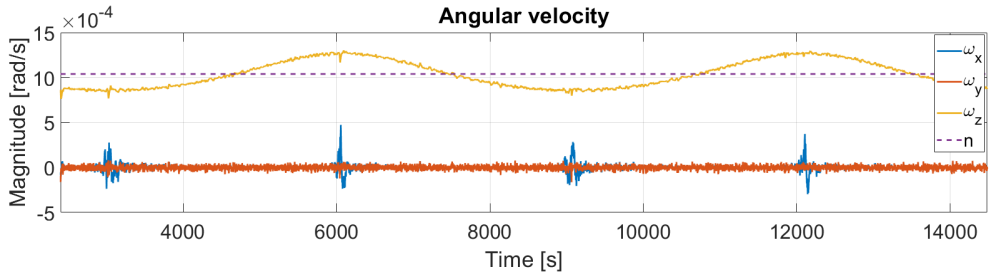

Figure 21: Angular velocity evolution during the Earth pointing phase.

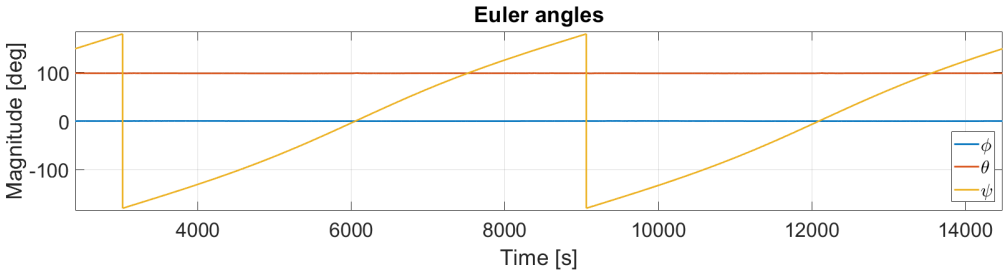

Figure 22: Euler's angles during Earth pointing phase.

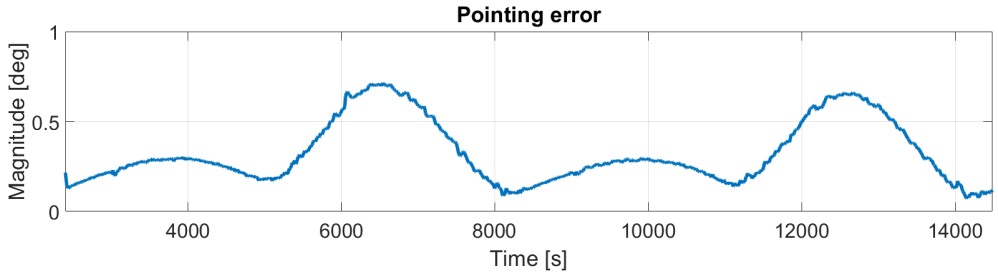

Figure 23: Pointing error during Earth pointing phase.

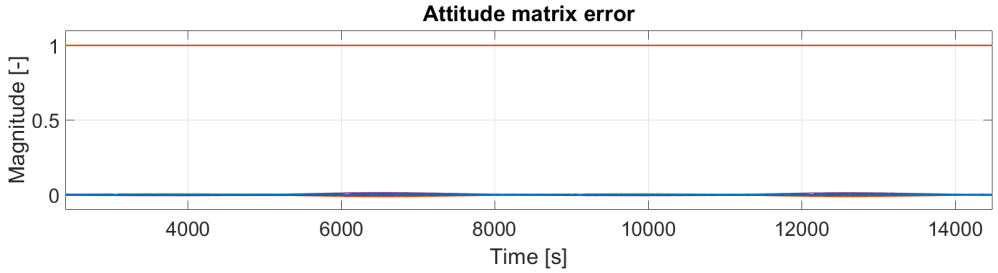

Figure 24: Attitude matrix error evolution during the Earth pointing phase.

Regarding the control torque, the real control momentum is reported in Figure 25, the difference between the real and ideal control torques is shown in Figure 26. At last, the thrust level for each actuator is plotted in Figure 27.

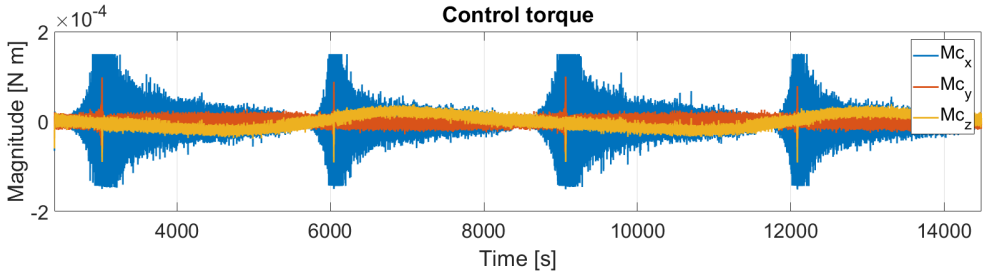

Figure 25: Control torque components during the Earth pointing phase.

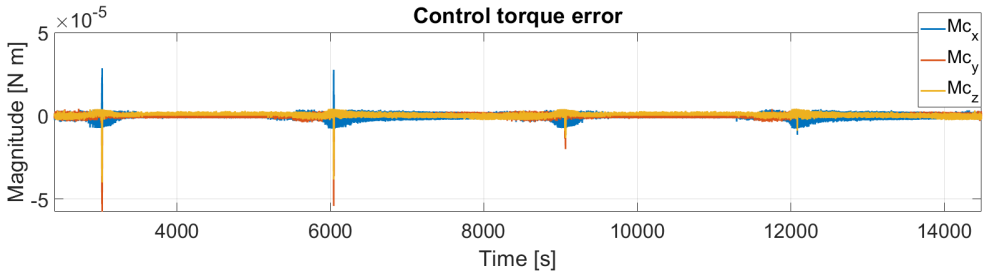

Figure 26: Ideal and real control torque differences during the Earth pointing phase.

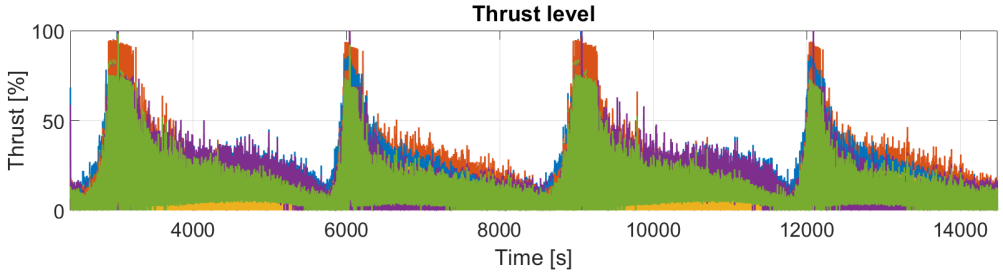

Figure 27: Thrust level during the Earth pointing phase.

7 Conclusions

The simulation results reported in the previous section prove that the ADC system designed satisfies the mission requirements of detumbling and Earth pointing expressed in Section 3. In addition, the performance parameter chosen, the pointing error, stays below the threshold value of 1° as wanted, and this is achieved using only variable thrust jets which simplifies the system. However, this choice generates the main drawback of this design, which is the long response time, in particular of the detumbling phase. It is possible to improve this by using more powerful actuators, such as control moment gyroscopes, or by using electric thruster with a wider thrust range.
The simulations of the system included all the main disturbances and dynamics, although it is possible to refine it, for example considering the small contribution of the atmospheric drag disturbing torque or using a more realistic magnetic model (choosing an higher order of the IGRF model), as well as considering the moving solar panels effects on the solar radiation pressure torque.

References

[1] Sensonor. *STIM300, Datasheet*. URL: https://sensonor.azurewebsites.net/media/5z5lv25o/ts1524-r27-datasheet-stim300.pdf.

[2] SolarMems Technologies. *nanoSSOC-D60, Datasheet*. URL: https://www.cubesatshop.com/wp-content/uploads/2016/06/nanoSSOC-D60-Technical-Specifications.pdf.

[3] Maryland Aerospace. *MAI-SES, Datasheet*. URL: https://www.cubesatshop.com/wp-content/uploads/2016/06/MAI-SES-Specifications-20150827.pdf.

[4] Enpulsion Spacecraft Technology. *NANO IR3, Datasheet*. URL: https://www.enpulsion.com/wp-content/uploads/ENP2020-078.A-NANO-IR3-Product-Overview.pdf.

[5] Franco Bernelli Zazzera. *Course notes, Spacecraft Attitude Dynamics and Control*.

[6] James Douglas Biggs. *Course notes, Spacecraft Attitude Dynamics and Control*.